Geochemical Perspectives Letters

Vivianite-parasymplesite solid solution: A sink for arsenic in ferruginous environments?

J.P.H. Perez[1*], M. Okhrymenko[1,†], R. Blukis[1,‡], V. Roddatis[1], S. Mayanna[1,§], J.F.W. Mosselmans[2], L.G. Benning[1,3]

https://doi.org/10.7185/geochemlet.2325

Abstract

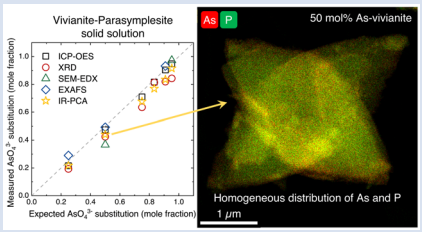

Vivianite, a hydrated ferrous phosphate [$Fe^{II}_3(PO_4)_2 \cdot 8\ H_2O$] that forms in oxygen-poor, but Fe^{2+}-rich conditions is important in nutrient cycling in anoxic environments. In natural vivianites, isomorphic substitution of divalent cations for structural Fe(II) are typical. However, anion substitution is rare; in particular, arsenate ($As^{V}O_4^{3-}$) substitution has never been documented in natural vivianites. Only partial substitution has been reported in synthetic analogues, and parasymplesite [$Fe^{II}_3(AsO_4)_2 \cdot 8\ H_2O$], the arsenic end member of the vivianite mineral group, is found in hydrothermal deposits. In this study, we detail structural changes in synthesised As-vivianites ($Fe^{II}_3[(PO_4)_{1-x}(AsO_4)_x]_2 \cdot 8\ H_2O$) with systematically increased degrees of As(V) substitution ($0.22 \leq x \leq 0.95$). As(V) was successfully incorporated into the vivianite crystal structure, creating a homogenous, solid solution between $As^{V}O_4^{3-}$ and PO_4^{3-}. Like both end members, the intermediate As-vivianites crystallised in the monoclinic system (*C*2/*m* space group), and retained the platelet crystal habit of As-free vivianite, even at the highest As(V) substitution. This uniform incorporation of As(V), and its replacement of PO_4^{3-}, provides a potentially stable sink for arsenic in anoxic soils and sediments, and may have implications in ferruginous early Earth oceans.

Received 24 January 2023 | Accepted 30 June 2023 | Published 3 August 2023

Introduction

Phosphorus is an essential nutrient that controls primary productivity in terrestrial and aquatic systems. Retention of phosphorus is strongly dependent on biomass uptake, mineral co-precipitation, or sorption onto mineral surfaces (Filippelli, 2002). In anoxic soils and sediments, reductive dissolution of Fe(III) (oxyhydr)oxides results in the release of dissolved phosphate (PO_4^{3-}) and Fe^{2+} (Patrick and Khalid, 1974), accompanied by increase to near neutral pH due to H^+ consumption (Walpersdorf *et al.*, 2013). Under anoxic, non-sulfidic (*i.e.* ferruginuous) conditions, high dissolved Fe^{2+} and PO_4^{3-} may lead to vivianite [$Fe^{II}_3(PO_4)_2 \cdot 8\ H_2O$] (Heiberg *et al.*, 2012) precipitation at near neutral pH. Vivianite can also form in aquatic ferruginous environments such as marine and lacustrine sediments and lakes (Egger *et al.*, 2015; Vuillemin *et al.*, 2020), and has been suggested as a potential phosphate sink in early Earth oceans (Hao *et al.*, 2020), affecting trace element cycling and nutrient availability.

Vivianite is the Fe(II) phosphate end member of the vivianite mineral group (monoclinic *C*2/*m*), represented by the general formula $M_3(YO_4)_2 \cdot 8\ H_2O$, where *M* refers to divalent cation(s) (*e.g.*, Fe(II), Mg, Mn) and *Y* can be either P or As. Vivianite is a poorly soluble mineral ($pK_{sp} \approx 35.8 \pm 0.08$ at 25 °C; Al-Borno and Tomson, 1994) that is stable under reducing and circum-neutral pH (6–9) conditions (Nriagu, 1972). Its structure has two crystallographically and chemically distinct Fe sites coordinated with phosphate (Fig. S-1): (i) a single octahedral Fe1 site [$FeO_2(H_2O)_4$)], and (ii) two edge sharing octahedral Fe2 sites [$Fe_2O_6(H_2O)_4$] (Mori and Ito, 1950; Bartl, 1989). These single and double edge sharing Fe octahedra are connected by tetrahedral phosphate to form layers in (010), interconnected by hydrogen bonds between lattice water molecules.

Isomorphic substitution of Fe^{2+} by divalent cations (*e.g.*, Mg, Mn) occurs frequently in natural vivianites, and although rarely documented, anions like arsenate (AsO_4^{3-}) can also replace PO_4^{3-} in the crystal structure (Muehe *et al.*, 2016). Anion substitution is possible because of chemical and structural similarities between phosphate and arsenate (*i.e.* geometry, size, pK_a). Full substitution of phosphate for arsenate results in a new phase, parasymplesite [$Fe^{II}_3(AsO_4)_2 \cdot 8\ H_2O$]. Contrary to vivianite, parasymplesite is usually found in oxidised zones of As-rich hydrothermal mineral deposits (Anthony *et al.*, 2000). Johnston and Singer (2007), however, predicted that parasymplesite can form in near neutral pH, reduced As-impacted groundwater (*e.g.*, Bangladesh), yet it has so far not been

1. GFZ German Research Center for Geosciences, Telegrafenberg, 14473 Potsdam, Germany
2. Diamond Light Source, Harwell Science and Innovation Campus, Didcot, Oxfordshire, OX11 0DE, United Kingdom
3. Department of Earth Sciences, Freie Universität Berlin, Malteserstrasse 74-100, 12249 Berlin, Germany
† Current affiliation: Department of Chemistry, RWTH Aachen University, 52056 Aachen, Germany
‡ Current affiliation: Leibniz-Institut für Kristallzüchtung (IKZ), Berlin 12489, Germany
§ Current affiliation: Carl Zeiss Microscopy GmbH, 73447 Oberkochen, Germany
* Corresponding author (Email: jpperez@gfz-potsdam.de)

reported. As(V)-substituted vivianite (~15 mol %; hereafter referred as As-vivianite) have been observed during microbial reduction of As(V)-bearing Fe(III) (oxyhydr)oxides (Muehe *et al.*, 2016), and such high As contents suggest a possible vivianite-parasymplesite solid solution. Thus, it is possible that As-vivianites are unrecognised possible host minerals and sinks for As in many anoxic environments.

To test this, we synthesised As-vivianites ($Fe_3[(PO_4)_{1-x}(AsO_4)_x]_2 \cdot 8\,H_2O$), with increasing degrees of AsO_4^{3-} substitution ($0.22 \leq x \leq 0.95$), under anoxic and near neutral pH conditions. Our results will help us better understand As dynamics in oxygen limited, Fe^{2+}-rich environments. We show that a continuous solid solution between vivianite and parasymplesite exist, and document how the structure, morphology and bonding environment of As-vivianite changes with increasing As(V) substitution. We also discuss how such a solid solution mineral system can be important in modern and ancient ferruginous, or contaminated environmental settings.

Materials and Methods

Co-precipitation experiments were conducted at room temperature in acid cleaned 120 mL perfluoroalkoxy (PFA) jars inside a vinyl-walled glovebox (97 % N_2, 3 % H_2). Stock solutions were prepared using deoxygenated ultrapure water (resistivity ~18.2 MΩ·cm), obtained by purging with argon at 90 °C for ~4 hr. Aliquots from stock solutions of 20 mM Na_2HAsO_4 and 20 mM Na_2HPO_4 (pH ~ 7) were mixed with ultrapure water to achieve desired AsO_4^{3-} mole fractions of 0.25, 0.50, 0.75, 0.83, 0.91 and 0.95 ($[AsO_4^{3-} + PO_4^{3-}] = 8$ mM). These were mixed with an aliquot of 0.58 M $Fe^{II}SO_4$ stock solution to achieve an $[Fe^{2+}]/[AsO_4^{3-} + PO_4^{3-}]$ ratio of 1.5 and pH ≈ 5. Precipitation was triggered by dropwise addition of 1 M NaOH, while stirring until pH 7.1 ± 0.2 was reached. Mineral suspensions were aged for 1 and 24 hr under constant stirring. End members, vivianite (no AsO_4^{3-}) and parasymplesite (no PO_4^{3-}) were also synthesised under similar conditions. Solids were collected by filtration, washed with deoxygenated ultrapure water, and subsequently dried, ground and stored in the glovebox until characterisation. The solutions and solids were characterised using inductively coupled plasma optical emission spectrometry (ICP-OES), powder X-ray diffraction (XRD), scanning and transmission electron microscopy (S/TEM), synchrotron-based X-ray absorption spectroscopy (XAS) and Fourier transform infrared (FTIR) spectroscopy. Detailed information on all characterisation methods and geochemical modelling can be found in Supplementary Text S-2.

Results and Discussion

Structure and composition of As-vivianites. The precipitates after 1 and 24 hr of aging were highly crystalline (Figs. 1a, S-2). All Bragg reflections could be assigned to vivianite or parasymplesite with no observable peak splitting, indicating homogeneity of the precipitates. No other crystalline Fe-P or Fe-As phases were present, and the similarity in the backgrounds in all patterns also suggest the lack of any amorphous phase contribution. The XRD results agree with our geochemical calculations (see saturation indices in Table S-2), which showed that vivianite and parasymplesite are the only thermodynamically stable phases in our system, irrespective of initial P:As ratios. The Eh-pH diagram of the Fe-P-As-H_2O system (Fig. S-4a) also clearly showed the overlapping predominance fields of vivianite and parasymplesite, and is well supported by the calculated mineral stability of the vivianite-parasymplesite solid solution (Fig. S-4b). Following the changes in concentration in the reacting solutions, it is clear that after 1 hr of aging, As and P removal was between 95 to 99 %, while Fe was less efficiently removed (80 to 96 %), revealing that the precipitated solids scavenged the phosphate and arsenate at a similar extent (Table S-3). The similarities and lack of differences between the 1 hr and aged solid phases led us to continue with the solid characterisations only on the 24 hr solids.

The gradual transition from a phosphate to an arsenate structure could be quantified from the XRD patterns, which showed slow structural transition from vivianite to parasymplesite with increasing AsO_4^{3-} mole fraction from 0.22 to 0.95 (Table S-4). These structural changes are evidenced by the displacement of the (100), ($\bar{2}$01), (310) and (201) vivianite reflections (dashed lines in Figs. 1a and S-2). As seen from the vivianite crystal structure model (Fig. S-1), these reflections correspond to lattice planes intersecting the interlinked Fe octahedra *via* PO_4^{3-} or AsO_4^{3-} tetrahedra, which expand at a higher degree of substitution because of the larger thermochemical radius of AsO_4^{3-} (2.48 Å) compared to PO_4^{3-} (2.38 Å) tetrahedra (Frausto da Silva and Williams, 2001). This is also reflected in the larger lattice parameters and associated cell volumes of As-vivianites (Fig. 1b–e) derived from Rietveld refinements (Table S-5, Fig. S-3), which increased linearly and suggest an isomorphous substitution following Vegard's law (Vegard, 1921). Lattice parameters *a*, *b* and *c* increased by 1 to 2 %, while the unit cell volume expanded up to 5 % compared to parasymplesite. The lattice parameters of natural vivianites, rarely occurring parasymplesite (only two refined structures exist in literature), and biogenic As-vivianites are also in agreement with the values obtained in this study (grey coloured symbols in Fig. 1b–e); although variations arising from natural heterogeneity (*e.g.*, partial substitution of Fe(II) sites by divalent cations, structural Fe(II) oxidation) exist in natural mineral specimens.

Morphology of As-vivianites and local distribution of P and As. The synthesised As vivianites (Figs. 2a, S-5a,b) exhibited large platy crystals (between 5–10 μm in length and 2–5 μm in width) elongated along the *a* axis direction and often radiating from the centre, similar to As-free vivianite (Fig. S-5c). In addition, all crystals in the vivianite-parasymplesite solid solution series were extremely thin, ranging from 50 to 100 nm, indicating slow growth of (010).

Mapping the elemental distribution of P and As in As-vivianites (*e.g.*, $x = 0.48$; Fig. 2b–d) by high angular dark field (HAADF) STEM imaging coupled with energy dispersive X-ray (EDX) mapping showed homogeneously distributed P and As in the crystals and no chemical zonation, even at higher magnification (Fig. S-6).

Further increasing the AsO_4^{3-} substitution even to $x = 0.95$, still resulted in plate-like crystals (Fig. S-5b). This is very different to the morphology of synthetic parasymplesite (*i.e.* As end member), which has a needle or lath-type crystal habit (0.5–5 μm in length and 0.5–2 μm in width; Fig. S-5d), indicating preferred crystal growth along the *c* axis. It is worth noting that synthetic As-vivianites had uneven crystal edges compared to synthetic As-free vivianite (Fig. S-5), and that vivianite and all As-vivianites, were extremely beam sensitive, degrading rapidly upon continuous exposure to electrons during imaging (*e.g.*, Fig. S-7).

Local bonding environment and speciation of Fe and As. Distinct features in the Fe K-edge EXAFS spectra clearly showed the gradual transition of Fe local bonding environment (yellow bands in Fig. 3a) with increasing AsO_4^{3-} substitution ($x = 0.22$, 0.48, 0.90). For example, the characteristic, prominent shoulders in the first and second oscillations at 5.2 and 8.0 $Å^{-1}$ in vivianite slowly decreased in intensity as AsO_4^{3-} substitution

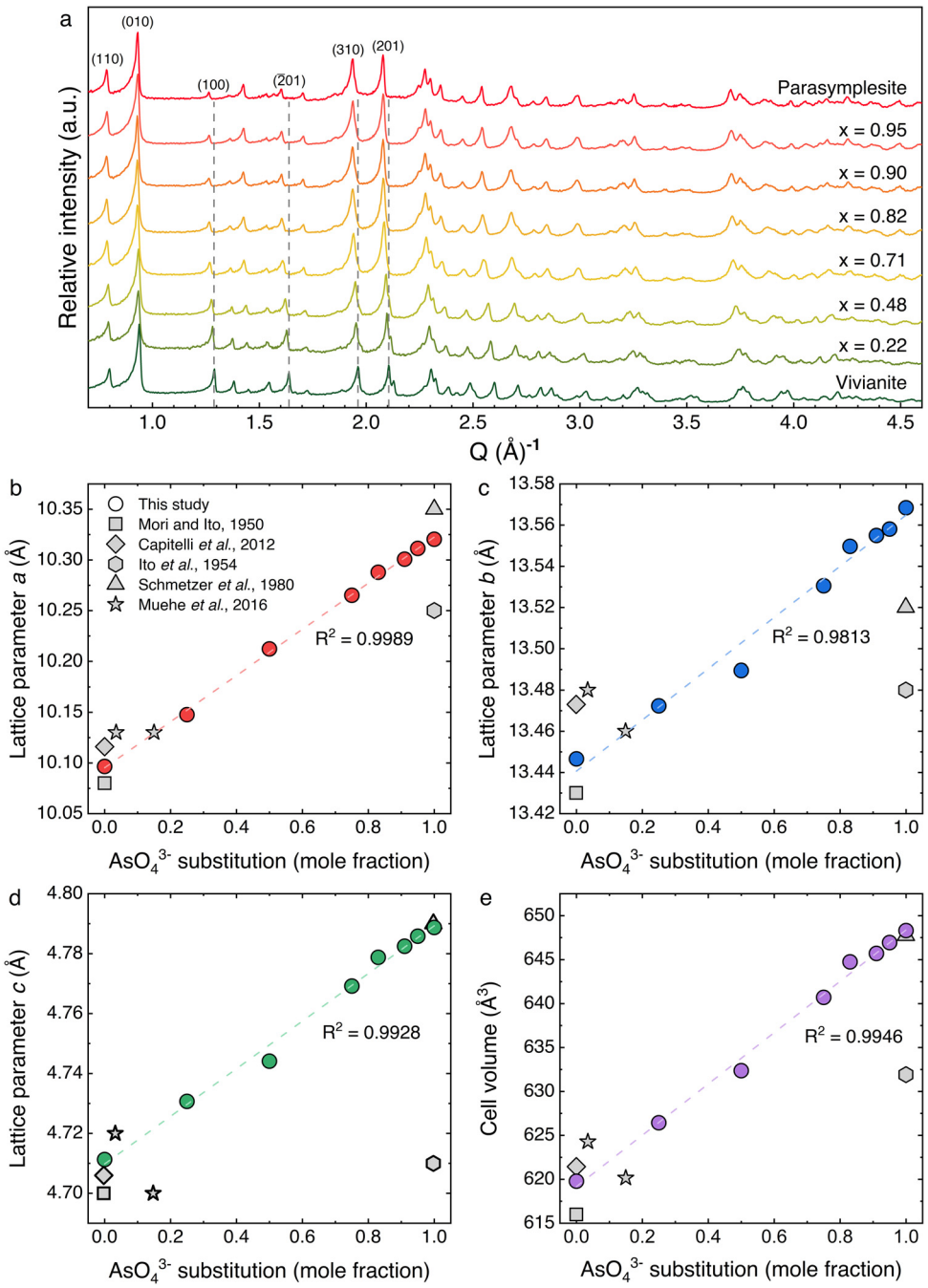

Figure 1 **(a)** XRD patterns of As-substituted vivianites (x = mole fraction of substituted AsO_4^{3-}) aged for 24 hr, plotted in Q-space ($Q = 2\pi/d_{hkl}$). Dashed grey lines indicate displacement in selected lattice planes in vivianite due to AsO_4^{3-} substitution for PO_4^{3-}. Full XRD patterns can be found in Figure S-2. Variations in lattice parameter values **(b–d)** and cell volumes **(e)** of our As-vivianites (coloured circles) compared to literature (Mori and Ito, 1950; Ito *et al.*, 1954; Schmetzer *et al.*, 1980; Capitelli *et al.*, 2012; Muehe *et al.*, 2016) shown as grey symbols. Dashed lines represent linear relationships as a function of As(V) substitution.

increased. Intense oscillations between 8.4 and 10 $Å^{-1}$ also dampened at 48 mol % AsO_4^{3-} substitution, and were replaced by a single oscillation at 90 mol % substitution as the Fe local bonding environment became more parasymplesite-like. The subtle beat feature found in parasymplesite at 7 $Å^{-1}$ only appeared at 90 mol % As(V) substitution (arrows in Fig. 3a). We could not perform shell-by-shell fits on the Fe K-edge EXAFS of As-vivianites because of the lack of spatial resolution required to fit multiple atomic pair paths (*i.e.* Fe-As, Fe-P) in the second shell. However, linear combination fitting (LCF) results of the Fe K-edge EXAFS spectra (Fig. 3b, Table S-6), in combination with our XRD Rietveld refinement, suggest that the Fe local bonding environment gradually changed from a vivianite-like to parasymplesite-like environment as As(V) substitution in the solids increased.

The As K-edge EXAFS spectrum of parasymplesite (topmost spectra; Fig. 3c) has pronounced shoulders in the first and second oscillations at 4.3 and 6.5 $Å^{-1}$, two beat features between 8 and 9 $Å^{-1}$ and a peak splitting in the third oscillation (arrows at $x = 0.90$ in Fig. 3c). These characteristic pronounced shoulders of parasymplesite can be seen in all As-vivianites, irrespective of degree of AsO_4^{3-} substitution. However, the two beat features and peak splitting in the third oscillation (arrows in Fig. 3c) only become apparent at high AsO_4^{3-}

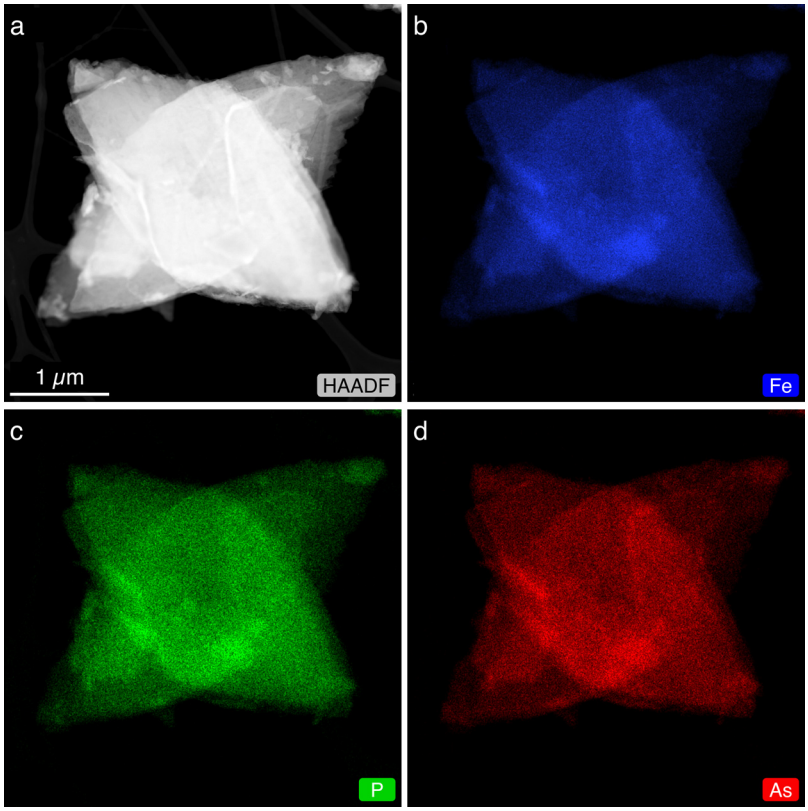

Figure 2 **(a)** HAADF-STEM image of As-substituted vivianite ($x = 0.48$) and corresponding EDX maps: **(b)** Fe (blue); **(c)** P (green); and **(d)** As (red).

substitution ($x \geq 0.90$). Nonetheless, shell-by-shell fitting (Fig. 3d, Table S-7) showed similarities in As local bonding environment in all As-vivianites and parasymplesite, even at low AsO_4^{3-} substitution ($x = 0.22$). In general, the first neighbour contribution to the EXAFS fit correspond to the As-O atomic correlation for tetrahedral AsO_4^{3-} ($R_{As\text{-}O} = 1.69$ Å); the second neighbour contribution arises from As-Fe atomic pairs of two corner-sharing linkages between AsO_4^{3-} tetrahedron and two Fe octahedra ($R_{As\text{-}Fe1} \approx 3.30$ Å, $R_{As\text{-}Fe2} \approx 3.47$ Å; Fig. S-8). These fit-derived interatomic distances are in excellent agreement with crystallographic values for parasymplesite (Mori and Ito, 1950), and are consistent with EXAFS-derived Fe-As distances in parasymplesite (Jönsson and Sherman, 2008).

More importantly, As(V) was not reduced by aqueous or structural Fe(II) during As-vivianite crystallisation. This is evident from the positions of the Fe and As K-edge X-ray absorption near edge structure (XANES) maxima of As-vivianites ($x = 0.22$, 0.48, 0.90) centred at 7,127 and 11,874 eV, respectively (Fig. S-9). These positions match the reference vivianite and parasymplesite, as well as other vivianites reported in literature (Miot *et al.*, 2009; Muehe *et al.*, 2016).

Our As K-edge EXAFS results are also supported by the FTIR data (Figs. 4, S-10), which confirmed increased AsO_4^{3-} substitution through gradually increasing intensities of $\nu(AsO_4)$ bands between ~885 and 700 cm^{-1} at the expense of $\nu(PO_4)$ bands between ~1120 and 885 cm^{-1} (Table S-8). The shoulder at ~792 cm^{-1} [$\nu(AsO_4)$] only appeared in the spectra of As-vivianite with >71 mol % substitution. At even higher AsO_4^{3-} substitution, a new band appeared at ~1076 cm^{-1} and the 1035 cm^{-1} band split into two component bands at 1042 and 1022 cm^{-1}, representing $\nu(PO_4)$ antisymmetric stretching modes (Makreski *et al.*, 2015). Substitution of AsO_4^{3-} in vivianite also affects the bonding environment of structural water; however, interpretation of the ν(OH) and δ(HOH) regions can be complicated (see further discussion in Supplementary Information S-2.5).

Naturally, the question arises whether As(V) is adsorbed to vivianite surfaces (*cf.* Thinnappan *et al.*, 2008), as in the case of other Fe(II)-bearing minerals. The As-Fe atomic distance for As(V) adsorbed as bidentate binuclear (^2C) and monodentate mononuclear (^1V) inner sphere surface complexes are $R_{As\text{-}Fe}$ of ~3.4 and ~3.5 Å, respectively (Jönsson and Sherman, 2008; Perez *et al.*, 2020), similar to our fit-derived distances for As-vivianites. We attempted to fit these two As-Fe paths to the second neighbour contribution of As-vivianites individually, but the fit yielded unrealistic CN values (*i.e.* negative, or extremely high CN values). To distinguish potentially adsorbed As(V) species in our As-vivianites, we reacted As(V) ($[As]_{initial} = 4$ mM) with pure vivianite ($[Fe]_{vivianite} = 12$ mM) at pH ~ 7 for 24 hr, comparable to the 48 mol % substituted As-vivianite. Structurally incorporated As would have resulted in shifts in vivianite reflections (*cf.* Fig. 1), but the XRD pattern of As-adsorbed vivianite was equivalent to the pure vivianite (Fig. S-11a). In addition, the $\nu(AsO_4)$ band in the FTIR spectrum (Fig. S-11b) of As-adsorbed vivianite only exhibited a very weak shoulder feature at ~780 cm^{-1} instead of the characteristic sharp bands seen in As-vivianites and parasymplesite (*cf.* Fig. 4). More importantly, adsorbed As(V) would not systematically decrease the intensities of $\nu(PO_4)$ bands in As-vivianites. SEM-EDX maps of As-adsorbed vivianite (Fig. S-12) also showed clear differences in As signal intensities and distribution compared to 48 mol % substituted As-vivianite (Fig. S-13). Overall, these results can be interpreted as arsenic being primarily structurally incorporated in As-vivianites, with only minor contributions from adsorbed species, if at all present.

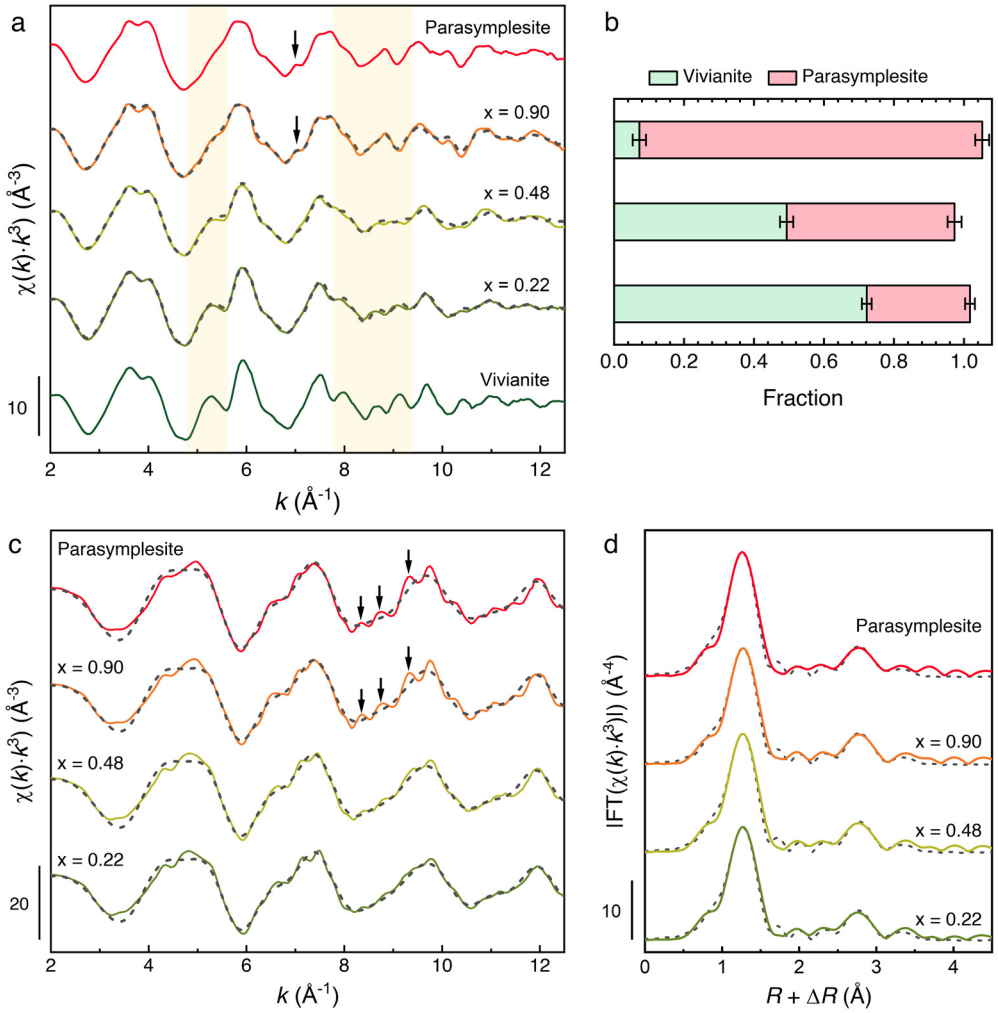

Figure 3 **(a)** Fe K-edge k^3-weighted EXAFS spectra of As-vivianites. Dashed grey lines denote **(b)** LCF of Fe K-edge EXAFS spectra of mineral end members (*i.e.* vivianite, parasymplesite). **(c)** As K-edge k^3-weighted EXAFS spectra of As vivianites and **(d)** corresponding Fourier transform magnitude. Dashed grey lines denote shell-by-shell fits.

Geochemical Implications

In this study, we explored the structural incorporation of As(V) in vivianite under anoxic conditions. Our complementary results (Fig. S-14) document and cross correlate that AsO_4^{3-} can systematically substitute for PO_4^{3-} in the vivianite crystal structure, thereby forming a continuous solid solution. We have showed that up to 95 mol % (~24 wt. %) of As(V) can be incorporated (Table S-4), with a very minor fraction of potentially adsorbed species. Sequestration of As(V) in vivianite *via* partial substitution for PO_4^{3-} under reduced conditions is favourable because most Fe(II)-bearing minerals have far lower As uptake, and sorption mechanisms are more susceptible to remobilisation upon desorption. Compared to interactions with other common Fe(II)-bearing minerals in ferruginous environments, where arsenic is primarily adsorbed and only reaches ~15 wt. % in magnetite (Yean *et al.*, 2005) or ~9 wt. % in green rust (Perez *et al.*, 2019), our current results show that arsenic incorporation into vivianite could be stable sinks for As(V) removal in ferruginous settings. For example, vivianite found in anoxic, non-sulfidic environments could incorporate major and trace elements (Vuillemin *et al.*, 2020; Kubeneck *et al.*, 2023). Therefore, As-vivianites may be present, yet so far undocumented in contaminated, anoxic settings such as in Bangladesh where vivianite and parasymplesite are both saturated (Johnston and Singer, 2007). However, since naturally occurring As-vivianites have yet to be found, their stability as a sink for arsenic under environmentally relevant conditions needs to be evaluated in further studies. In addition to the potential importance of As-vivianites in contaminated settings, our findings have implications for phosphorus

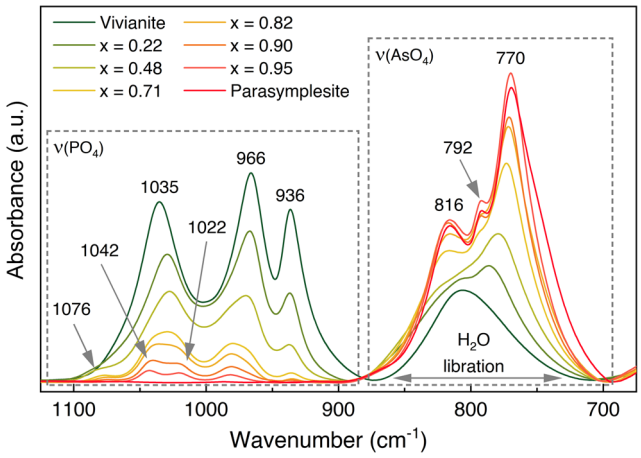

Figure 4 FTIR spectra of As(V)-substituted vivianites showing stretching regions for phosphate [$\nu(PO_4)$] and arsenate [$\nu(AsO_4)$], and H_2O libration vibrations. Full spectra and band assignments can be found in Figures S-10 and Table S-8, respectively.

(and arsenic) cycling since vivianite has been suggested as a P sink in Precambrian oceans (Hao *et al.*, 2020), and modern lake analogues (Xiong *et al.*, 2019; Vuillemin *et al.*, 2020). Given the widespread occurrence of arsenate in these ancient oceans (Chi Fru *et al.*, 2016), As(V) substitution for P in vivianites would have reduced the bioavailability of toxic As species, and could have shaped how life emerged and adapted in the Precambrian oceans (Visscher *et al.*, 2020).

Acknowledgements

This project has received funding from the European Union's Horizon 2020 Marie Skłodowska-Curie Innovative Training Network METAL-AID (grant no. 675219), Helmholtz Recruiting Initiative awarded to LGB (award no. I-044-16-01), GFZ expedition fund (grant no. X-044-20-01) for support for travel to the synchrotron facility, and Deutsche Forschungsgemeinschaft (DFG, German Research Foundation) "Open Access Publikationskosten" funding programme (project no. 491075472). JPHP acknowledges the Royal Society of Chemistry (RSC) for the Researcher Development Grant (grant no. D22-2132977309). MO was funded by the Förderverein Chemie-Olympiade (FChO) during her research internship. ICP-OES analyses were carried out at the Helmholtz Laboratory for the Geochemistry of the Earth Surface (HELGES) at GFZ Potsdam. The authors especially thank the European Development Fund and the state of Brandenburg for the Themis Z S/TEM, a part of the Potsdam Imaging and Spectral Analysis (PISA) Facility at GFZ Potsdam. SEM-EDX maps of the As-adsorbed vivianite were collected with the help of Marcin Daniel Syczewski. We acknowledge Diamond Light Source for time on I20-scanning beamline under proposal SP23496-1, with thanks to Shu Hayama for assistance. We also like to thank Dominique J. Tobler and Thaïs Couasnon for their help during beamtime.

Editor: Juan Liu

Additional Information

Supplementary Information accompanies this letter at https://www.geochemicalperspectivesletters.org/article2325.

Cite this letter as: Perez, J.P.H., Okhrymenko, M., Blukis, R., Roddatis, V., Mayanna, S., Mosselmans, J.F.W., Benning, L.G. (2023) Vivianite-parasymplesite solid solution: A sink for arsenic in ferruginous environments? *Geochem. Persp. Let.* 26, 50–56. https://doi.org/10.7185/geochemlet.2325

References

Al-Borno, A., Tomson, M.B. (1994) The temperature dependence of the solubility product constant of vivianite. *Geochimica et Cosmochimica Acta* 58, 5373–5378. https://doi.org/10.1016/0016-7037(94)90236-4

Anthony, J.W., Bideaux, R.A., Bladh, K.W., Nichols, M.C. (2000) *Handbook of Mineralogy Volume IV: Arsenates, Phosphates and Vanadates*. Mineral Data Publishing, Tucson, Arizona, USA.

Bartl, H. (1989) Water of crystallization and its hydrogen-bonded crosslinking in vivianite $Fe_3(PO_4)_2 \cdot 8H_2O$; a neutron diffraction investigation. *Fresenius' Zeitschrift für analytische Chemie* 333, 401–403. https://doi.org/10.1007/BF00572335

Capitelli, F., Chita, G., Ghiara, M.R., Rossi, M. (2012) Crystal-chemical investigation of $Fe_3(PO_4)_2 \cdot 8\,H_2O$ vivianite minerals. *Zeitschrift für Kristallographie - Crystalline Materials* 227, 92–101. https://doi.org/10.1524/zkri.2012.1442

Chi Fru, E., Arvestål, E., Callac, N., El Albani, A., Kilias, S., Argyraki, A., Jakobsson, M. (2016) Arsenic stress after the Proterozoic glaciations. *Scientific Reports* 5, 17789. https://doi.org/10.1038/srep17789

Egger, M., Jilbert, T., Behrends, T., Rivard, C., Slomp, C.P. (2015) Vivianite is a major sink for phosphorus in methanogenic coastal surface sediments. *Geochimica et Cosmochimica Acta* 169, 217–235. https://doi.org/10.1016/j.gca.2015.09.012

Filippelli, G.M. (2002) The Global Phosphorus Cycle. In: Kohn, M.J., Rakovan, J., Hughes, J.M. (Eds.) *Phosphates: Geochemical, Geobiological, and Materials Importance*. Reviews in Mineralogy and Geochemistry 48, 391–425. https://doi.org/10.2138/rmg.2002.48.10

Frausto da Silva, J.J.R., Williams, R.J.P. (2001) *The Biological Chemistry of the Elements: The Inorganic Chemistry of Life*. Oxford University Press, Oxford.

Hao, J., Knoll, A.H., Huang, F., Schieber, J., Hazen, R.M., Daniel, I. (2020) Cycling phosphorus on the Archean Earth: Part II. Phosphorus limitation on primary production in Archean ecosystems. *Geochimica et Cosmochimica Acta* 280, 360–377. https://doi.org/10.1016/j.gca.2020.04.005

Heiberg, L., Koch, C.B., Kjaergaard, C., Jensen, H.S., Hansen, H.C.B. (2012) Vivianite Precipitation and Phosphate Sorption following Iron Reduction in Anoxic Soils. *Journal of Environmental Quality* 41, 938–949. https://doi.org/10.2134/jeq2011.0067

Ito, T.-i., Minato, H., Sakurai, K.'i. (1954) Parasymplesite, a New Mineral Potymorphous with Symplesite. *Proceedings of the Japan Academy* 30, 318–324. https://doi.org/10.2183/pjab1945.30.318

Johnston, R.B., Singer, P.C. (2007) Solubility of Symplesite (Ferrous Arsenate): Implications for Reduced Groundwaters and Other Geochemical Environments. *Soil Science Society of America Journal* 71, 101–107. https://doi.org/10.2136/sssaj2006.0023

Jönsson, J., Sherman, D.M. (2008) Sorption of As(III) and As(V) to siderite, green rust (fougerite) and magnetite: Implications for arsenic release in anoxic groundwaters. *Chemical Geology* 255, 173–181. https://doi.org/10.1016/j.chemgeo.2008.06.036

Kubeneck, L.J., ThomasArrigo, L.K., Rothwell, K.A., Kaegi, R., Kretzschmar, R. (2023) Competitive incorporation of Mn and Mg in vivianite at varying salinity and effects on crystal structure and morphology. *Geochimica et Cosmochimica Acta* 346, 231–244. https://doi.org/10.1016/j.gca.2023.01.029

Makreski, P., Stefov, S., Pejov, L., Jovanovski, G. (2015) Theoretical and experimental study of the vibrational spectra of (para)symplesite and hornesite. *Spectrochimica Acta Part A: Molecular and Biomolecular Spectroscopy* 144, 155–162. https://doi.org/10.1016/j.saa.2015.01.108

Miot, J., Benzerara, K., Morin, G., Bernard, S., Beyssac, O., Larquet, E., Kappler, A., Guyot, F. (2009) Transformation of vivianite by anaerobic nitrate-reducing iron-oxidizing bacteria. *Geobiology* 7, 373–384. https://doi.org/10.1111/j.1472-4669.2009.00203.x

Mori, H., Ito, T. (1950) The Structure of Vivianite and Symplesite. *Acta Crystallographica* 3, 1–6. https://doi.org/10.1107/S0365110X5000001X

Muehe, E.M., Morin, G., Scheer, L., Le Pape, P., Esteve, I., Daus, B., Kappler, A. (2016) Arsenic(V) Incorporation in Vivianite during Microbial Reduction of Arsenic (V)-Bearing Biogenic Fe(III) (Oxyhydr)oxides. *Environmental Science & Technology* 50, 2281–2291. https://doi.org/10.1021/acs.est.5b04625

Nriagu, J.O. (1972) Stability of vivianite and ion-pair formation in the system $Fe_3(PO_4)_2$-H_3PO_4-H_2O. *Geochimica et Cosmochimica Acta* 36, 459–470. https://doi.org/10.1016/0016-7037(72)90035-X

Patrick Jr., W.H., Khalid, R.A. (1974) Phosphate Release and Sorption by Soils and Sediments: Effect of Aerobic and Anaerobic Conditions. *Science* 186, 53–55. https://doi.org/10.1126/science.186.4158.53

Perez, J.P.H., Freeman, H.M., Schuessler, J.A., Benning, L.G. (2019) The interfacial reactivity of arsenic species with green rust sulfate (GR_{SO4}). *Science of The Total Environment* 648, 1161–1170. https://doi.org/10.1016/j.scitotenv.2018.08.163

Perez, J.P.H., Freeman, H.M., Brown, A.P., van Genuchten, C.M., Dideriksen, K., S'Ari, M., Tobler, D.J., Benning, L.G. (2020) Direct Visualization of Arsenic Binding on Green Rust Sulfate. *Environmental Science & Technology* 54, 3297–3305. https://doi.org/10.1021/acs.est.9b07092

Schmetzer, K., Tremmel, G., Bartelke, W. (1980) Eine Paragenese seltener Minerale aus Bou-Azzer, Marokko: Parasymplesit, Symplesit, Schneiderhöhnit, Karibibit. *Neues Jahrbuch für Mineralogie - Abhandlungen* 138, 94–108.

Thinnappan, V., Merrifield, C.M., Islam, F.S., Polya, D.A., Wincott, P., Wogelius, R.A. (2008) A combined experimental study of vivianite and

As (V) reactivity in the pH range 2–11. *Applied Geochemistry* 23, 3187–3204. https://doi.org/10.1016/j.apgeochem.2008.07.001

Vegard, L. (1921) Die Konstitution der Mischkristalle und die Raumfüllung der Atome. *Zeitschrift für Physik* 5, 17–26. https://doi.org/10.1007/BF01349680

Visscher, P.T., Gallagher, K.L., Bouton, A., Farias, M.E., Kurth, D., Sancho-Tomás, M., Philippot, P., Somogyi, A., Medjoubi, K., Vennin, E., Bourillot, R., Walter, M.R., Burns, B.P., Contreras, M., Dupraz, C. (2020) Modern arsenotrophic microbial mats provide an analogue for life in the anoxic Archean. *Communications Earth & Environment* 1, 24. https://doi.org/10.1038/s43247-020-00025-2

Vuillemin, A., Friese, A., Wirth, R., Schuessler, J.A., Schleicher, A.M., Kemnitz, H., Lücke, A., Bauer, K.W., Nomosatryo, S., von Blanckenburg, F., Simister, R., Ordoñez, L.G., Ariztegui, D., Henny, C., Russell, J.M., Bijaksana, S., Vogel, H., Crowe, S.A., Kallmeyer, J., the Towuti Drilling Project Science team (2020) Vivianite formation in ferruginous sediments from Lake Towuti, Indonesia. *Biogeosciences* 17, 1955–1973. https://doi.org/10.5194/bg-17-1955-2020

Walpersdorf, E., Bender Koch, C., Heiberg, L., O'Connell, D.W., Kjaergaard, C., Bruun Hansen, H.C. (2013) Does vivianite control phosphate solubility in anoxic meadow soils? *Geoderma* 193–194, 189–199. https://doi.org/10.1016/j.geoderma.2012.10.003

Xiong, Y., Guilbaud, R., Peacock, C.L., Cox, R.P., Canfield, D.E., Krom, M.D., Poulton, S.W. (2019) Phosphorus cycling in Lake Cadagno, Switzerland: A low sulfate euxinic ocean analogue. *Geochimica et Cosmochimica Acta* 251, 116–135. https://doi.org/10.1016/j.gca.2019.02.011

Yean, S., Cong, L., Yavuz, C.T., Mayo, J.T., Yu, W.W., Kan, A.T., Colvin, V.L., Tomson, M.B. (2005) Effect of magnetite particle size on adsorption and desorption of arsenite and arsenate. *Journal of Materials Research* 20, 3255–3264. https://doi.org/10.1557/jmr.2005.0403